SINGLE IMAGE HAZE REMOVAL BASED ON SALIENCY DETECTION AND DARK CHANNEL PRIOR

Libao Zhang, Xiaohan Wang and Chen She*

College of Information Science and Technology, Beijing Normal University, Beijing 100875, China

ABSTRACT

Since more and more outdoor images are often degraded by haze and suffer from bad visibility, which includes low contrast, low resolution, and high luminance, haze removal has become an important task of image restoration in recent years. In this paper, we propose a saliency prior, which introduces human visual attention mechanism into haze removal. The prior reveals the relationship between the saliency analysis and the depth of hazy scenes. In our dehazing method, firstly, saliency map and salient regions are obtained. Then, an accurate airlight and a refined transmission map can be acquired based on saliency prior and dark channel prior. Finally, we can restore the haze-free image successfully using the airlight and the transmission map. Experimental results show that our method performs much better than others in recovering large white areas that are inherently similar to the airlight.

Index Terms—Image restoration, haze removal, salient detection, dark channel prior, transmission refinement.

1. INTRODUCTION

Nowadays, since more and more images taken in outdoor conditions suffer from bad visibility because of the degradation of haze, haze removal has become an indispensable step when we deal with these degraded images in computer vision applications. Considering that human visual attention mechanism can still work well in a bad weather such as fog and haze, it is meaningful to introduce human attention mechanism into haze removal.

Several approaches have been proposed for dehazing in recent years. Some methods need multiple images or additional information of the same scene [1-7]. Others try to remove haze with single image by different assumptions. Fattle et al. [8] assumed that surface shading and scene transmission are locally uncorrelated. Tan et al. [9] removed haze component by assuming that haze-free images have higher contrast than images plagued by haze. He et al. [10] proposed dark channel prior to simplify the problem. Based on dark channel prior, some dehazing algorithms were further proposed. Tarel et al. [11] achieved fast haze removal using median filter. Meng et al. [12] restored a high quality image with fine details benefiting from boundary constraint and contextual regularization.

Saliency detection is an attractive topic of human visual attention mechanism [13-15]. Koch and Ullman [16] firstly introduced the concept of the saliency map. Then, Itti proposed a visual attention model [17] to generate the final saliency map by weighted fusion of conspicuity maps of color, intensity, and orientation. Some purely computational models are also proposed, including the spectral residual presented by Hou et al. [18], and the model using wavelet transform presented by Imamoglu et al [19]. Recently, researchers' attention has been drawn by some region-based methods. Shi et al. [20] proposed a hierarchical saliency detection model. Cheng et al. [21] presented a region contrast based model for saliency detection.

Dark channel prior has drawn much attention since it was proposed in [10], which performs pretty well in restoring outdoor images with thin fog. However, it cannot handle the hazy images with large white objects that are inherently similar to the atmospheric light. And though many methods were proposed to improve the efficiency and details of DCP, this problem has not been solved well so far.

(a) (b) (c) (d) (e)

Fig. 1. *Result comparison of different dehazing methods. (a) Original image; (b) He's result [10]; (c) Tarel's results [11]; (d) Meng's results [12]; (e) Our results.*

In this paper, we propose a saliency prior to help solve the above problem. The prior reveals the relationship between the saliency and the depth of hazy scenes. Combining saliency detection with dark channel prior, we can obtain an accurate airlight and a refined transmission map, which help to restore the haze-free image. As illustrated in Fig. 1, when dealing with hazy images with large white areas, especially when the area is an object that is inherently similar to the airlight, the results of previous methods look over-saturated and unnatural. Our method performs well in both color and saturation restoring.

*Corresponding author: libaozhang@163.com. This research was supported by National Natural Science Foundation of China (61571050 and 61071103) and Beijing Natural Science Foundation (4162033).

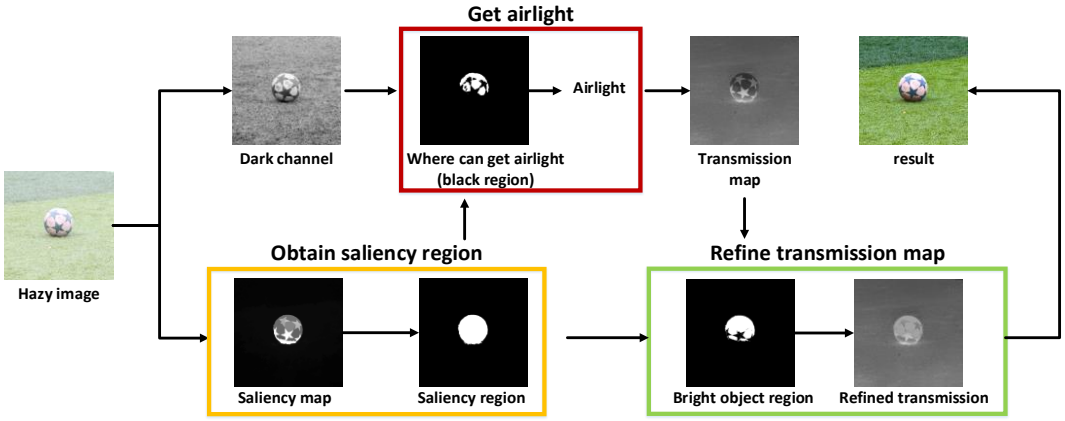

Fig. 2. *The framework of the proposed method.*

2. METHODOLOGY

In this section, we introduce our method of recovering images with large white regions. The structure of our method is shown in Fig. 2. First, we obtain the saliency map and the salient region. Then, accurate airlight is acquired based on saliency prior and dark channel prior. After that, the saliency prior is used again to refine the transmission map obtained by dark channel prior. Ultimately, we can recover the haze-free image by combining airlight and transmission map.

2.1 Saliency prior

Generally, the formation of a hazy image can be described as the follow equation [3, 9, 10]:

$$I(x) = J(x) * t(x) + A(1 - t(x)) \qquad (1)$$

where x is a pixel coordinate, I is the observed intensity, J is the scene radiance without haze, A is the global atmospheric light, and t is the medium transmission describing the portion of light that is not scattered and reaches the camera. Since the atmosphere is supposed to be homogenous, the transmission t can be expressed as:

$$t(x) = e^{-\beta d(x)} \qquad (2)$$

where β is the scattering coefficient of atmosphere and d is the scene depth. Equation (2) means that $t(x)$ is attenuated exponentially with the depth [10].

Salient regions often show high local contract with their surrounding regions in luminance, color, and orientation. But in a hazy image, because of the degradation of turbid medium, remote objects cannot show these characteristics, which means salient regions cannot exist in a region where $d(x)$ is large. Therefore, when a local region is salient, the region should be close to the camera, which means it is an object instead of dense haze. Besides, since salient region tends to be one object, $d(x)$ of the region is usually the same. Based on equation (2), it can be inferred that the transmission is also the same in the region.

According to the above analysis, the saliency prior can be concluded as: there is always an object rather than opaque haze in the salient region and the region has the same transmission everywhere.

2.2 Salient region detection

In our model, we adopt hierarchical saliency detection [17] to obtain saliency maps of hazy images. Then, 0.1 is used as a threshold value to gain a binary image, in which white regions represent salient regions. The reason why we choose 0.1 is to filter little background out of the final results. Fig. 3 shows the saliency maps and salient regions of different images.

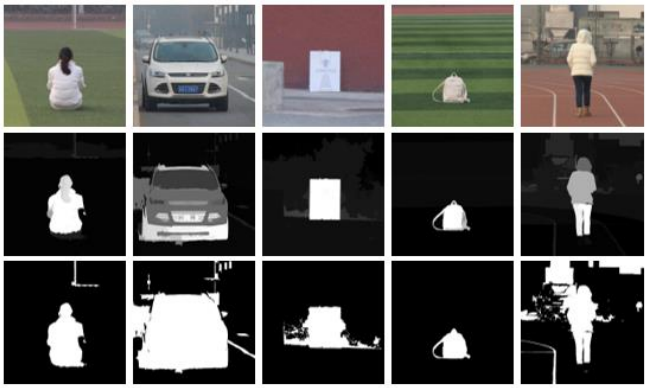

Fig. 3. *Saliency maps and salient regions. Top: Original images; Middle: Saliency maps; Bottom: Salient regions.*

2.3 Atmospheric light

In dark channel prior [10], He et al. firstly get dark channel J^{dark} by

$$J^{dark}(x) = \min_{y \in \Omega(x)} \left(\min_{c \in \{r,g,b\}} J^c(y) \right) \qquad (3)$$

where J^c is a color channel of J and $\Omega(x)$ is a local patch centered at x. Then, he estimated atmospheric light by the highest intensity of the most haze-opaque region, whose pixels are the top 0.1 percent brightest ones in the dark channel, in order to avoid some brightest pixels that are

brighter than airlight, such as a white car. However, as shown in Fig. 4, this method still will select inaccurate pixels when dealing with a white object that is larger than the patch size.

In our method, we introduce saliency detection into dark channel prior to minimize the influence of large white objects. Based on our observation of hazy images, we find that in dark channel, the most haze-opaque regions often are about 0.7, and regions that have a value greater than it tend to be sky and other large white objects. Since salient region must be objects, by finding salient pixels whose value are greater than 0.7 in dark channel and excluding them from where we get airlight, we can greatly lower the influence of these white objects when obtaining the atmospheric light. We compare our airlight results with He's in Table 1.

Fig. 4. *The dark channels of images with large white objects (1024×1024) using 15×15 patches for different images.*

Table 1. *The airlight of input images in Fig. 3 obtained by He's method in [10] and ours method in RGB space.*

Image	He's method			Our method		
(1)	0.967	0.934	0.955	0.768	0.754	0.788
(2)	0.844	0.852	0.862	0.758	0.766	0.759
(3)	0.841	0.866	0.957	0.773	0.818	0.919
(4)	0.885	0.849	0.848	0.820	0.771	0.745
(5)	0.943	0.912	0.844	0.889	0.834	0.735

2.4 Transmission map

In [10], He et al. observed $J^{dark} \to 0$ in most local patches in haze-free images. Therefore, He estimated the transmission map simply by

$$\tilde{t}(x) = 1 - \omega \min_{y \in \Omega(x)} (\min_{c} \frac{I^c(y)}{A^c}) \tag{4}$$

where ω is a constant parameter between 0 and 1 to optionally keep a very small amount of haze for the remote objects. Then this transmission map can be further refined by soft matting [10] or guided filter [22, 23].

However, it cannot satisfy $J^{dark} \to 0$ apparently when dealing with white objects that are larger than the patch size. Under such conditions, equation (4) will fail since the regions of these objects have a high value in the dark channel, which means they are considered to be the most haze-opaque regions and the transmission is estimated much lower than its true value. To overcome the above disadvantage of dark channel prior, in this paper, we use saliency prior to refine the transmission map obtained by He's method.

Firstly, we find the white area by a comparison between the intensity and the airlight in each channel from RGB space:

$$W = \{x : \min_{c \in \{r,g,b\}} (I^c - \lambda A^c) \geq 0\} \tag{5}$$

where W is the white area, and λ is a constant parameter between 0 and 1. In this paper, we fix λ to 0.6, which means a pixel can be considered as a white pixel if its intensity is greater than 60 percent of airlight in each RGB channel. The white region obtained by this step contains both white objects and opaque haze regions.

Since the transmission of haze-opaque region can be estimated correctly by equation (4), where the transmission map needs to be refined is the white object region:

$$N = W \bigcap S \tag{6}$$

where N is the region needs to be refined, and S is the salient region.

Based on the saliency prior that the salient region usually has the same transmission everywhere, the incorrect transmission value can be replaced by another normal value in the transmission map of the salient region:

$$t(x) = t_s \quad (x \in N) \tag{7}$$

where t_s is the transmission value that the salient region should have. Since pixels with low intensities have more accurate transmission, and their transmission is relatively large according to equation (4), in our method, we firstly list all the transmission in the salient region in a descending order, and then choose the smallest one that is larger than 85 percent of the values in the order as t_s. 85 percent is chosen experimentally and it can avoid some highest transmission that is very close to one, which occurs in a few pixels occasionally. The comparison of our transmission map and He's is in Fig. 5.

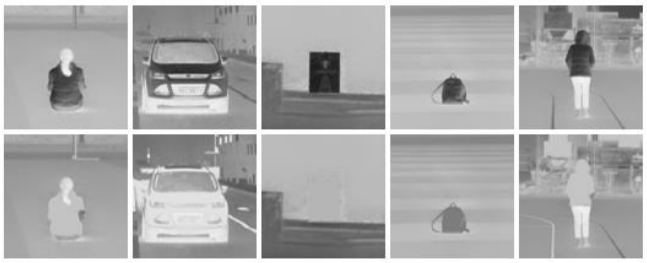

Fig. 5. *Comparison of the transmission maps of He's method in [10] (first row) and our method (second row).*

2.5 Haze-free image

According to [10], with the atmospheric light and the refined transmission map, the haze-free image can be estimated by

$$J(x) = \frac{I(x) - A}{\max(t(x), t_0)} + A \tag{8}$$

where t_0 is a lower bound for the transmission $t(x)$ to prevent the directly recovered scene radiance J being prone to noise when $t(x)$ is close to zero. The typical value of t_0 is 0.1.

3. EXPERIMENTAL RESULTS

In this section, we compare our results with the results of He et al. [10], Tarel et al. [11], and Meng et al. [12] when dealing with images with large white objects. The comparison includes qualitative and quantitative evaluation.

3.1 Qualitative comparison

In Fig. 6, we show the comparison of results of different dehazing methods when dealing with images with large white region. We can easily notice that the results of He and Tarel show a wrong color in the white area, since they estimated the depth of these areas incorrectly. Besides, though Meng's work performs well in restoring the color of white region, the whole image looks over-saturated and unnatural. By contrast, our method recovers the color of white region successfully while keeping the background haze-removed and natural.

(a) (b) (c) (d) (e)

Fig. 6. *Result comparison of four dehazing methods. (a) Original image; (b) He's result [10]; (c) Tarel's results [11]; (d) Meng's results [12]; (e) Our results.*

3.2 Quantitative comparison

We use the indicators proposed in [24] to evaluate the results of these four methods, where e represents the rate of new visible edges, $\bar{r}$ denotes the quality of contrast restoration, and σ expresses the rate of saturated pixels. Table 2 shows that these four methods perform almost the same in increasing visible edges. Table 3 indicates that Tarel and Meng do a better job than He and us in contrast restoration. Since the images we use have large white region, σ is supposed to be an appropriate value instead of as low as possible. Therefore, as shown in Table 4, our method performs much better than the others in this indicator.

Table 2. *Indicator e of the images in Fig. 6.*

e	He	Tarel	Meng	Our
First row	3.43	3.83	3.14	3.33
Second row	1.85	2.26	1.53	1.64
Third row	1.7178	2.7205	1.0272	1.6312
Fourth row	12.23	7.28	8.35	12.99
Fifth row	2.17	2.46	2.02	1.95

Table 3. *Indicator $\bar{r}$ of the images in Fig. 6.*

$\bar{r}$	He	Tarel	Meng	Our
First row	1.24	2.01	2.64	1.42
Second row	1.09	2.48	3.39	1.28
Third row	1.3449	2.4669	3.7351	1.3707
Fourth row	1.32	2.17	2.21	1.37
Fifth row	1.19	1.95	1.81	1.24

Table 4. *Indicator σ of the images in Fig. 6.*

σ	He	Tarel	Meng	Our
First row	0.0002%	0	0.0009%	0.0015%
Second row	0.0090%	0	0.0123%	0.1566%
Third row	0.0031%	0	0.0094%	0.0257%
Fourth row	0	0	0	0
Fifth row	0.0001%	0	0.0818%	0.0184%

3.3 Discussion

As illustrated in Fig. 6, our method mainly focuses on recovering the color of large white region, thus it performs better in qualitative comparison and indicator σ, while having no advantages on the other two indicators.

In some cases, the salient region contains several objects whose depth is not the same. Besides, the constant parameters we are using now are not fit every different images. We leave these problems for future research.

4. CONCLUSION

In this paper, we proposed a saliency prior, which revealed the relationship between the saliency and the depth of hazy scenes. With saliency prior and dark channel prior, we can obtain an accurate airlight and a refined transmission map, which help to restore the haze-free images. Experimental results show that the proposed method performs much better in recovering both color and saturation of large white objects than dark channel prior and other dehazing methods.

5. REFERENCES

[1] Y.Y Schechner, S.G. Narasimhan, and S.K. Nayar, "Instant dehazing of images using polarization," *2001 IEEE Conference on Computer Vision and Pattern Recognition (CVPR)*, vol. 1, pp. 325-332, 2001.

[2] S. Shwartz, E. Namer, and Y.Y. Schechner, "Blind haze separation," *2006 IEEE Conference on Computer Vision and Pattern Recognition (CVPR)*, vol. 2, pp. 1984-1991, 2006.

[3] B. Cai, X. Xu, K. Jia, C. Qing, and D. Tao, "DehazeNet: An end-to-end system for single image haze removal," *IEEE Transactions on Image Processing*, vol. 25, no. 11, pp. 5187-5198, 2016.

[4] Z. Li, and J. Zheng, "Edge-preserving decomposition-based single image haze removal," *IEEE Transactions on Image Processing*, vol. 24, no. 12, pp. 5432-5441, 2015.

[5] X. Pan, F. Xie, Z. Jiang, and J. Yin, "Haze removal for a single remote sensing image based on deformed haze imaging model," *IEEE Signal Processing Letters*, vol. 22, no. 10, pp. 1806-1810, 2015.

[6] Q. Zhu, J. Mai, and L. Shao, "A fast single image haze removal algorithm using color attenuation prior," *IEEE Transactions on Image Processing*, vol. 24, no. 11, pp. 3522-3533, 2015.

[7] S.G. Narasimhan and S.K. Nayar, "Contrast restoration of weather degraded images," *IEEE Transactions on Pattern Analysis and Machine Intelligence*, vol. 25, no. 6 pp. 713-724, 2003.

[8] B. Li, S. Wang, J. Zheng, and L. Zheng, "Single image haze removal using content-adaptive dark channel and post enhancement," *IET Computer Vision*, vol. 8, no. 2, pp. 131-140, 2014.

[9] R. Tan, "Visibility in bad weather from a single image," *2008 IEEE Conference on Computer Vision and Pattern Recognition (CVPR)*, pp. 1-8, June 2008.

[10] K. He, J. Sun, and X. Tang, "Single image haze removal using dark channel prior," *IEEE Transactions on Pattern Analysis and Machine Intelligence*, vol. 33, no 12, pp. 2341-2353, Dec. 2011.

[11] J. P. Tarel and N. Hautiere, "Fast visibility restoration from a single color or gray level image," *2009 IEEE International Conference on Computer Vision (ICCV)*, pp. 2201-2208, 2009.

[12] G. Meng, Y. Wang, J. Duan, S. Xiang, and C. Pan, "Efficient image dehazing with boundary constraint and contextual regularization," *2013 IEEE International Conference on Computer Vision (ICCV)*, pp. 617-624, Dec. 2013.

[13] L. Zhang, A. Li, Z. Zhang, and K. Yang, "Global and local saliency analysis for the extraction of residential areas in high-spatial-resolution remote sensing image," *IEEE Transactions on Geoscience and Remote Sensing*, vol. 54, no. 7, pp. 3750-3763, 2016.

[14] L. Zhang and K. Yang, "Region-of-interest extraction based on frequency domain analysis and salient region detection for remote sensing image," *IEEE Geoscience and Remote Sensing Letters*, vol. 11, no. 5, pp. 916-920, 2014.

[15] L. Zhang, K. Yang, and H. Li, "Regions of interest detection in panchromatic remote sensing images based on multiscale feature fusion," *IEEE Journal of Selected Topics in Applied Earth Observations and Remote Sensing*, vol. 7, no. 12, pp. 4704-4716, 2014.

[16] C. Koch and S. Ullman, "Shifts in selective visual attention: towards the underlying neural circuitry," *Human Neurobiology,* vol. 4, no. 4, pp. 219-227, 1985.

[17] L. Itti, C. Koch, and E. Niebur, "A model of saliency-based visual attention for rapid scene analysis," *IEEE Transactions on Pattern Analysis and Machine Intelligence*, vol. 20, no. 11, pp. 1254-1259, 1998.

[18] X. Hou and L. Zhang, "Saliency detection: A spectral residual approach," *2007 IEEE Conference on Computer Vision and Pattern Recognition (CVPR)*, pp. 1-8, 2007.

[19] N. Imamoglu, W. Lin, and Y. Fang, "A saliency detection model using low-level features based on wavelet transform," *IEEE Transactions on Multimedia*, vol. 15, no. 1, pp. 96-105, 2013.

[20] J. Shi, Q. Yan, L. Xu, and J. Jia, "Hierarchical image saliency detection on extended CSSD," *IEEE Transactions on Pattern Analysis and Machine Intelligence*, vol. 38, no. 4, pp. 717-729, 2016.

[21] M. Cheng, N. Mitra, X. Huang, P. Torr and S. Hu, "Global contrast based salient region detection," *IEEE Transactions on Pattern Analysis and Machine Intelligence*, vol. 37, no. 3, pp. 569-582, 2015.

[22] K. He, J. Sun, and X. Tang, "Guided image filtering," *IEEE Transactions on Pattern Analysis and Machine Intelligence*, vol. 35, no. 6, pp. 1397-1409, 2013.

[23] Z. Li, J. Zheng, Z. Zhu, W. Yao, and S. Wu, "Weighted guided image filtering," *IEEE Transactions on Image Processing*, vol. 24, no. 1, pp. 120-129, 2015.

[24] N. Hautiere, J.P. Tarel, D. Aubert, and E. Dumont, "Blind contrast enhancement assessment by gradient ratioing at visible edges," *Image Analysis & Stereology Journal*, vol. 27, no. 2, pp. 87-95, 2008.